A Model for the Boreal Summer Intraseasonal Oscillation

BIN WANG AND XIAOSU XIE*

Department of Meteorology, University of Hawaii, Honolulu, Hawaii

ABSTRACT

The tropical intraseasonal oscillation (ISO) exhibits pronounced seasonality. The boreal summer ISO is more complex than its winter counterpart due to the coexistence of equatorial eastward, off-equatorial westward, and northward propagating, low-frequency modes and their interactions. Based on observational evidence and results obtained from numerical experiments, a mechanism is proposed for the boreal summer ISO in which the Northern Hemisphere summer monsoon (NHSM) circulation and moist static energy distribution play essential roles.

With a climatological July mean basic state, the life cycle of model low-frequency waves consists of four processes: an equatorial eastward propagation of a coupled Kelvin–Rossby wave packet, an emanation of moist Rossby waves in the western Pacific, a westward propagation and amplification of the Rossby waves in South Asian monsoon regions, and a reinitiation of the equatorial disturbances over the central Indian Ocean. The life cycle spans about one month and provides a mechanism for self-sustained boreal summer ISO.

Analyses of the model experiments reveal that the monsoon mean flows and spatial variation of moist static energy trap equatorial disturbances in the NHSM domain. The reduction of moist static energy over the eastern central Pacific suppresses equatorial convection, leading to disintegration of the equatorial Kelvin–Rossby wave packet and the emanation of Rossby waves in the western North Pacific. Strong easterly vertical shears and seasonally enhanced boundary layer humidity in the NHSM further amplify the Rossby waves (of the gravest meridional mode), making their structures highly asymmetric about the equator. The intensified Rossby waves start to stall and decay when approaching the Arabian Sea due to the ''blocking'' of the sinking dry air mass over North Africa, meanwhile triggering equatorial convection. The mean Hadley circulation plays a critical role in reinitiation of the equatorial Kelvin–Rossby wave packet over the equatorial Indian Ocean.

1. Introduction

Tropical intraseasonal oscillations (ISOs) display considerable seasonal variations in their intensity, frequency, and movement. The Madden–Julian oscillation (MJO) originally described by Madden and Julian (1971, 1972) is an equatorial eastward propagating mode, predominantly wavenumber one in zonal wind. Madden (1986) found that the zonal wind anomaly on the 40–50 day timescale exceeds that in adjacent lower- and higher-frequency bands by the largest amount during boreal winter. The oscillation period was found to change from 50 days in boreal winter to about 35 days in boreal summer over the Indian Ocean region (Hartmann et al. 1992). The MJO mode dominates the intraseasonal variability in boreal winter from November to April, yet it is notably weaker in boreal summer from May to October, during which events of northward and westward propagations occur more frequently (Wang and Rui 1990a; Hendon and Salby 1994). Pronounced seasonality is one of the fundamental features of the tropical intraseasonal oscillation.

The boreal summer ISO is considerably more complicated than its winter counterpart. The complexity lies in the coexistence of three types of propagating low-frequency modes: the MJO mode, the northward propagating mode over the Indian and western North Pacific monsoon regions (e.g., Yasunari 1979, 1981; Krishnamurti and Sabrahmanyam 1982; Chen and Murakami 1988), and the off-equatorial westward propagating mode (Murakami 1980). In addition, the boreal summer ISO exhibits a significant standing component between the equatorial Indian Ocean and the tropical western North Pacific (Zhu and Wang 1993). The different modes appear to interact with each other. Statistically, the equatorial Indian Ocean stands out as a preferred inception and intensification region for the intraseasonal convective anomalies; the western North Pacific is another active area of boreal summer intraseasonal variability; in contrast, the Maritime Continent and equatorial eastern central Pacific are regions of dissipation (Wang and Rui 1990a).

The westward propagating mode has received less

* Current Affiliation: Jet Propulsion Laboratory, California Institute of Technology, Pasadena, California.

Corresponding author address: Dr. Bin Wang, Department of Meteorology, University of Hawaii, 2525 Correa Road, Honolulu, HI 96822.
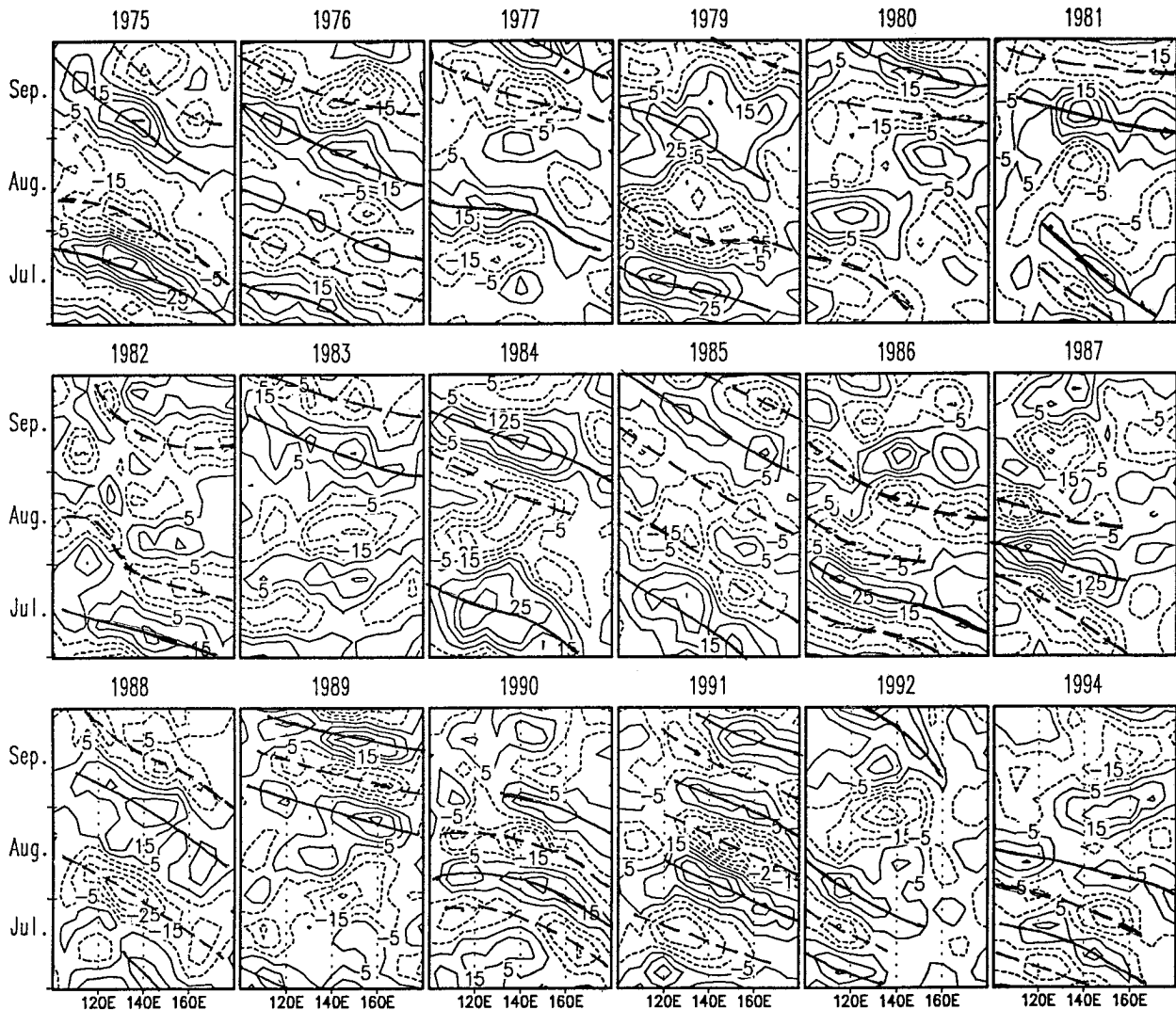
E-mail: bwang@soest.hawaii.edu

FIG. 1. Time–longitude diagrams of bandpass-filtered 20–72-day OLR anomalies averaged over the latitude bands between 12.5° and 22.5°N during July, August, and September for 1975–94 (1978 and 1993 missing). Contour interval is 10 Wm^{-2}. Negative OLR anomalies are dashed. Thick solid (dashed) lines outline westward propagation of positive and negative OLR anomalies.

attention in the literature and deserves more discussion here. Murakami (1980) and Murakami et al. (1984) presented evidence of 20–30 day perturbations propagating westward along 10°–20°N west of the date line, using both OLR and wind data. Wang and Rui (1990a), based on an analysis of 10 years of pentad mean OLR anomaly maps, identified the primary tracks of the westward-moving intraseasonal convective anomalies. Typical westward phase speed is 5 m s^{-1} and the zonal wavelength is about 4000 to 6000 km. As shown in Fig. 1, on 20–72 day timescale, the OLR anomalies exhibit prevailing westward propagations along 15°N from the western Pacific to the Bay of Bengal during July, August, and September. Although the westward propagation is sometimes episodic and has prominent year-to-year variations, it is, nevertheless, a predominant mode in the off-equatorial monsoon regions.

It is interesting that the westward propagating disturbances were found often to originate from the equatorial western Pacific. Using satellite-observed high cloud amount data, Nitta (1987) found that the cloud anomalies move eastward from the equatorial Indian Ocean to the western Pacific, then turn sharply northwestward and afterward move westward along 10°–20°N (Fig. 11 of Nitta). The behavior of the westward propagating vorticity waves with a wavelength of 4000 km and a speed of about 5 m s^{-1} was documented in detail by Lau and Lau (1990). Their teleconnectivity map of the bandpass-filtered 850-hPa relative vorticity field (Fig. 5 of Lau and Lau 1990) show a clear propagation track which starts from the equatorial western Pacific and turns toward South Asian summer monsoon regions. Figure 16 of Murakami et al. (1984) presented a good example of the horizontal structure and westward

propagation of this type of disturbances. Although individual waves have a synoptic-scale lifespan, the wave activity is regulated on a 30–40 day timescale.

A number of theoretical and numerical studies have attempted to explain aspects of the boreal summer ISO. Most of them focus on the cause of the northward propagation on a timescale of 20–40 days in the Indian monsoon region. Webster (1983) emphasized the key role of the land surface heat fluxes into the boundary layer that destabilizes the atmosphere ahead of the ascending zone and causes a northward shift of the convective zones. On the other hand, Goswami and Shukla (1984) stressed the role of a convection–thermal relaxation feedback in the northward propagation: convective activity results in an increase of static stability which depresses convection itself; meanwhile, dynamic and radiative relaxation decreases moist static stability and brings the atmosphere to a new convectively unstable state. Lau and Peng (1990), based on their numerical experiments, suggested that the interaction of equatorial Kelvin waves with large-scale monsoon mean flows can generate unstable quasigeostrophic baroclinic waves with period of 5–6 days over the Indian monsoon region along 15°–20°N; meanwhile the equatorial disturbances weaken.

Whereas observations have documented the complicated behavior of the boreal summer ISO, the physical processes associated with the westward propagation and the preferred development of low-frequency disturbances over the equatorial Indian Ocean and western North Pacific remain unexplained. Given the fact that the low-frequency wave activity in boreal summer is strongly confined to the Northern Hemisphere (NH) tropical monsoon domain, we postulate that the large-scale monsoon mean flows and the moisture distribution might have fundamental impacts on the structure, propagation, and development of low-frequency disturbances and the maintenance of the tropical ISO.

The present study is aimed at testing this idea and developing our understanding of the dynamics of boreal summer ISO, in particular, the effects of spatial variations of planetary-scale monsoonal flows on the behavior of low-frequency equatorial waves. Specific questions to be addressed include the following: (1) Why is the western North Pacific a preferred region for generation of westward propagating disturbances and the equatorial Indian Ocean a preferred region for recurrence or inception of the eastward-moving disturbances? (2) How are the westward propagating, low-frequency waves initiated, intensified, and dissipated? (3) What role does the monsoon circulation play in sustaining the boreal summer ISO?

An intermediate tropical atmospheric model with a steady, three-dimensional basic state is used for modeling boreal summer ISO and presented in section 2. Section 3 describes results of the control experiment, which reveal how the realistic July mean circulation and moist static energy distribution regulate transient wave activity in the model. In sections 4 and 5, we further investigate the effects of mean monsoonal flows and moist static energy distribution on equatorial waves and the primary processes that are responsible for the simulated life cycle of boreal summer low-frequency wave activities. The last section presents a summary and discusses limitations of the model.

2. The model

The model used in this study is an extension of the model for intraseasonal oscillation developed by Wang and Li (1994). The latter belongs to the category of intermediate models. The original model contains only basic equatorial wave dynamics interacting with tropical boundary layer processes and parameterized convective heating. Without including mean flows, the model was capable of qualitatively reproducing several essential features of the MJO mode, such as the dominant slow equatorial eastward propagation, the gross baroclinic vertical structure, the close association of convective anomalies with low-level westerly anomalies, the near-equatorial zonal wind and off-equatorial rotational circulations, the longitudinal dependence for the strength, and the multispatial scales: large-scale convective complex systems coupled with planetary-scale circulation systems (Wang and Li 1994). The present model extends that model by including three-dimensional steady basic flows.

a. Model equations

The low-frequency perturbation motion in the free troposphere satisfies the following linearized primitive equations in a p coordinate, equatorial β plane:

$$\frac{\partial u'}{\partial t} = -\bar{u}\frac{\partial u'}{\partial x} - u'\frac{\partial \bar{u}}{\partial x} - \bar{v}\frac{\partial u'}{\partial y} - v'\frac{\partial \bar{u}}{\partial y}$$
$$- \bar{\omega}\frac{\partial u'}{\partial p} - \omega'\frac{\partial \bar{u}}{\partial p} + \beta y v' - \frac{\partial \phi'}{\partial x}$$
$$- \epsilon u' + K\nabla^2 u', \qquad (2.1a)$$

$$\frac{\partial v'}{\partial t} = -\bar{u}\frac{\partial v'}{\partial x} - u'\frac{\partial \bar{v}}{\partial x} - \bar{v}\frac{\partial v'}{\partial y} - v'\frac{\partial \bar{v}}{\partial y} - \bar{\omega}\frac{\partial v'}{\partial p}$$
$$- \omega'\frac{\partial \bar{v}}{\partial p} - \beta y u' - \frac{\partial \phi'}{\partial y} - \epsilon v' + K\nabla^2 v', \quad (2.1b)$$

$$\frac{\partial T'}{\partial t} = -\bar{u}\frac{\partial T'}{\partial x} - u'\frac{\partial \bar{T}}{\partial x} - \bar{v}\frac{\partial T'}{\partial y} - v'\frac{\partial \bar{T}}{\partial y}$$
$$+ \frac{p}{R}\bar{S}\omega' + \frac{p}{R}S'\bar{\omega} + \frac{Q'}{C_p} - \mu T' + K\nabla^2 T',$$

$$\qquad (2.1c)$$

$$\frac{\partial u'}{\partial x} + \frac{\partial v'}{\partial y} + \frac{\partial \omega'}{\partial p} = 0, \qquad (2.1d)$$

$$\frac{\partial \phi'}{\partial p} = -\frac{RT'}{p}, \qquad (2.1e)$$

where overbar and prime denote basic-state and perturbation quantities, respectively; u, v, ω, ϕ, and T denote zonal and meridional winds, vertical pressure velocity, geopotential, and temperature, respectively; ϵ and μ are the Rayleigh friction and Newtonian cooling coefficients, respectively; K the horizontal momentum or thermal diffusion coefficient; and S the dry static stability parameter. A standard 2-level free atmospheric model can be established by writing momentum and continuity equations at the upper- and lower-tropospheric levels of p_1 and p_2 and the thermodynamic and hydrostatic equations at level $p_m = 2^{-1}(p_1 + p_2)$.

The condensational heating rate due to deep convection is parameterized on the basis of the moisture and heat budget, following Kuo (1974). At the level p_m, it is expressed as (Wang 1988)

$$Q'_m = \frac{\delta b L_c}{\Delta p}[-\omega'_m(\bar{q}_2 - \bar{q}_1) - \omega'_e(\bar{q}_e - \bar{q}_2)], \quad (2.2)$$

where the heating switch-on function $\delta = H(Q'_m)$ is unity as $Q'_m > 0$ and zero as $Q'_m < 0$, representing the irreversible nature of the condensational heating; b measures the ratio of the amount of water vapor that condenses out to that moistening the atmosphere; L_c is the latent heat; Δp is the half-depth of the free atmosphere; ω'_m and ω'_e represent vertical pressure velocities at p_m and the top of the boundary layer p_e, respectively; and $\bar{q}_e$, $\bar{q}_2$, and $\bar{q}_1$ are vertical mean specific humidity of the basic state in the boundary layer, the lower and upper troposphere, respectively. The basic-state absolute humidity is assumed to decay exponentially with height, so that the vertical distribution of moisture content is solely determined by the surface specific humidity $\bar{q}_s$. Wang (1988) showed that the vertical mean specific humidity in a layer between p_i and p_j ($p_j > p_i$) is given by

$$\bar{q}(p_i, p_j) = \bar{q}_s \frac{p_j^m - p_i^m}{m(p_j - p_i)}, \quad (2.3)$$

where $m = H/H_1$; H and H_1 are air density and water vapor density scale height, respectively. The basic state $\bar{q}_s$ varies spatially and measures the moist static energy source available for perturbations. Although inclusion of the perturbation surface evaporation E'_v is trivial, it has been neglected because E'_v associated with intraseasonal waves is an order of magnitude smaller than the perturbation precipitation rate (Lau et al. 1988) and our sensitivity test indicates that its effect on unstable waves is small in the present diabatic heating formulation (Wang and Li 1994). With other model formulations, the perturbation evaporation may have a significant contribution to the circulation change (Emanuel 1987; Raymond 1994).

The boundary layer is described by a barotropic model. For large-scale, low-frequency tropical motion, the momentum balance approximately holds among the pressure gradient force, Coriolis force, and a Rayleigh friction that represents the friction and the high-fre-

quency transient eddy effects. The governing equations take the form

$$\beta y v'_B - \frac{\partial \phi'_e}{\partial x} - E_x u'_B = 0, \quad (2.4a)$$

$$-\beta y u'_B - \frac{\partial \phi'_e}{\partial y} - E_y v'_B = 0, \quad (2.4b)$$

$$\omega'_e = (p_s - p_e)\left(\frac{\partial u'_B}{\partial x} + \frac{\partial v'_B}{\partial y}\right), \quad (2.4c)$$

where p_s is pressure at the model surface; ϕ'_e represents perturbation geopotential at p_e; u'_B and v'_B are vertically averaged perturbation zonal and meridional winds in the boundary layer; and E_x and E_y are Rayleigh friction coefficients in the zonal and meridional directions. This specific form of horizontal momentum damping can be derived in different ways for the vertically averaged boundary layer flows (e.g., Wang 1988). Diagnostic studies using observed monthly mean surface pressure and winds indicated that in order to apply (2.4) to the time mean flow (neglecting the Reynolds stress due to high frequency disturbances) the Rayleigh friction coefficients should be anisotropic: E_y is generally two or three times as large as E_x (Wang and Li 1993). The mean flow terms in (2.4a) and (2.4b) were neglected because sensitivity tests show that the removal of these terms does not affect the results as long as the dissipation timescale is on an order of one day.

From Eq. (2.4), the Ekman pumping velocity is

$$\omega'_e = D_1 \frac{\partial^2 \phi'_e}{\partial x^2} + D_2 \frac{\partial \phi'_e}{\partial x} + D_3 \frac{\partial^2 \phi'_e}{\partial y^2} + D_4 \frac{\partial \phi'_e}{\partial y}, \quad (2.5)$$

where the coefficients are

$$D_1 = -\frac{(p_s - p_e)E_y}{E_x E_y + \beta^2 y^2},$$

$$D_2 = \frac{(p_s - p_e)\beta}{E_x E_y + \beta^2 y^2} - \frac{2(p_s - p_e)\beta^3 y^2}{(E_x E_y + \beta^2 y^2)^2},$$

$$D_3 = -\frac{(p_s - p_e)E_x}{E_x E_y + \beta^2 y^2},$$

$$D_4 = \frac{2(p_s - p_e)E_x \beta^2 y}{(E_x E_y + \beta^2 y^2)^2}.$$

Note that ω'_e is related to free atmosphere convergence by mass conservation in a vertical column:

$$\omega'_e = -\Delta p \sum_{k=1}^{2}\left(\frac{\partial u'_k}{\partial x} + \frac{\partial v'_k}{\partial y}\right). \quad (2.6)$$

Combining (2.5) and (2.6) leads to an elliptical equation for ϕ'_e:

TABLE 1. Model parameters.

p_e	Pressure at the top of the boundary layer	900 hPa
p_t	Pressure at the top of the free atmosphere	100 hPa
ϵ	Rayleigh friction coefficient	1.5×10^{-6} s^{-1}
μ	Newtonian cooling coefficient	1.5×10^{-6} s^{-1}
E_x	Dissipation coefficient in the boundary layer	3×10^{-5} s^{-1}
K	Horizontal diffusion coefficient	5×10^{5} m^2 s^{-1}
b	Precipitation efficiency coefficient	0.9
S_m	Mean static stability parameter at the middle level	3×10^{-6} m^2 s^{-2} Pa^{-2}
m	Density scale height/water vapor density scale height	3.45

$$D_1 \frac{\partial^2 \phi_e'}{\partial x^2} + D_2 \frac{\partial \phi_e'}{\partial x} + D_3 \frac{\partial^2 \phi_e'}{\partial y^2} + D_4 \frac{\partial \phi_e'}{\partial y}$$

$$= -\Delta p \sum_{k=1}^{2} \left(\frac{\partial u_k'}{\partial x} + \frac{\partial v_k'}{\partial y} \right). \qquad (2.7)$$

Equations (2.1) and (2.7) form a closed set of equations with the approximation of $\phi_e' = \phi_2'$.

b. Numerical scheme

The model is confined to an equatorial β channel between 40°S and 40°N. A parallel model in spherical coordinates is also developed to check the validity of the equatorial β plane approximation (see Wang and Xie 1996). The results obtained from two models are quite comparable for the numerical experiments performed in the present study. The zonal boundary condition is periodic around the globe. At the meridional boundaries the fluxes of mass, momentum, and heat normal to the boundaries vanish. A number of model parameters used in the numerical calculations are listed in Table 1.

Finite differences are used in both space and time. The spatial grid box is 5° longitude by 2° latitude and the time step is 10 min. Sensitivity tests are performed using a finer spatial grid size. The results show that the horizontal circulation structures are not sensitive to the change in grid size, although phase speed is slightly reduced and the growth rate slightly increases. To solve the elliptic equation (2.7), a Fourier transform is applied in the zonal direction with a truncation of one-fourth of the zonal grid points. Finite differencing is used in the meridional direction. Thus, for each wavenumber, an equation with y derivatives can be obtained and solved by matrix inversion.

c. Basic states

The model mean flow is the climatological July mean circulation which is derived from the European Centre for Medium-Range Weather Forecasts (ECMWF) gridded analysis data for the period 1979–92. The 200- and 850-hPa winds are used as the mean winds at the upper and lower levels of the model. The mean temperature at the midlevel was determined from geopotential thickness between 200 and 850 hPa by assuming a hydrostatic balance. The vertical p velocity at the midlevel is consistent with the mass continuity determined by the given wind field. The mean monsoon circulation is characterized by an upper-level anticyclone overlaying a low-level cyclone over South Asia (Figs. 2a,b). Distinguished from other seasons, a strong tropical easterly jet is formed in the upper troposphere over the northern Indian Ocean. At 850 hPa, strong westerlies prevail north of the equator in connection with cross-equatorial flow. Prominent vertical shears are fundamental characteristics of the monsoon circulation which delineates the strength and intensity of the summer monsoon (Webster and Yang 1992) (Fig. 2c).

In the model, the free atmospheric moisture content of the basic state depends only on the specific humidity at the surface. The latter is calculated based on surface air temperature and dewpoint temperature from the ECMWF data for July with proper smoothing to emphasize large-scale features (Fig. 3a). In order to identify the effects of the zonal and meridional variations of the moist static energy on the model ISO, we constructed a symmetric moisture field (Fig. 3b) that is the symmetric component of Fig. 3a and a zonally uniform moisture field (Fig. 3c), which is obtained by taking the zonal mean of the symmetric field between 80°–100°E.

3. The life cycle of low-frequency disturbances in the model

In order to examine the evolution of the model low-frequency disturbances during boreal summer, a control experiment (expt 1) is first performed with the climatological July mean flow (Fig. 2) and the July mean surface specific humidity (Fig. 3a) as the model's basic state. An initial perturbation with a circular shape and a diameter of 4000 km is centered at 40°E on the equator. The wind perturbation is purely zonal and has a cosine shape in both the zonal and meridional directions. The geopotential and temperature fields are determined by semigeostrophic and hydrostatic balances.

Snapshots of horizontal structure for the lower-tropospheric winds and precipitation rate are shown in Fig. 4. The upper-tropospheric winds are 180° out of phase with the lower-tropospheric winds. In the beginning the disturbance moves eastward along the equator, as its major component is an equatorial Kelvin wave (Fig. 4a). Since the boundary layer generates meridional flows that affect convective heating, the disturbance soon involves both Kelvin and Rossby wave components. By day 4 the perturbation develops a precipitation complex consisting of an equatorial cell and two off-equatorial cells, indicating that the perturbation becomes a combined equatorial Kelvin–Rossby wave packet coupled by convective heating [figure not shown, for more dis-

July

(a) 200 hPa   —20.0 m/s

(b) 850 hPa   —10.0 m/s
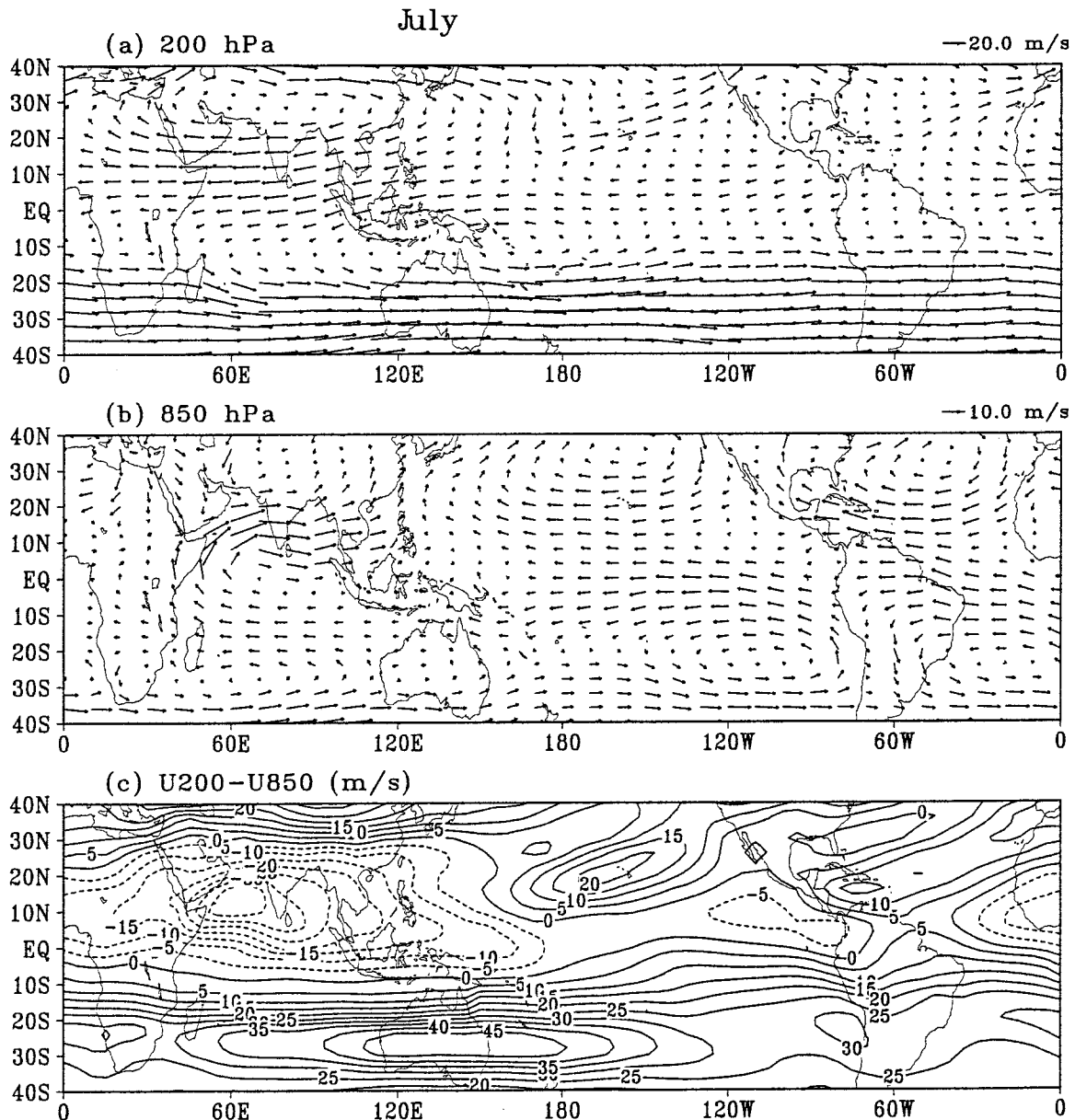

(c) U200−U850 (m/s)

FIG. 2. The climatological July mean winds at (a) 200 hPa and (b) 850 hPa. (c) The vertical shear of the July mean zonal flow defined by the difference $U_{200}-U_{850}$. The data were derived from ECMWF global analyses for the period 1979–92.

cussion see Wang and Li (1994)]. The off-equatorial westward propagating cells are associated with lower-level cyclonic vortices and have a typical zonal scale of 2000–4000 km. They originate from the eastward-migrating precipitation complex (Fig. 4b).

When the precipitation complex arrives at the western Pacific at day 10, it reintensifies and starts to emit convective cells northwestward toward the Indian monsoon region (Fig. 4c). At day 14, the equatorial disturbance reaches the central Pacific and attenuates; meanwhile, two large-scale vortices interacting with convective heating develop over the Arabian Sea and the South China Sea–Philippines area, respectively (Fig. 4d). The

former decays after day 16, whereas the latter further intensifies during its westward journey (Fig. 4e).

The characteristic structure and propagation suggest that the westward propagating disturbances are the gravest meridional mode of moist Rossby waves destabilized and modified by the monsoon easterly shear. Xie and Wang (1996) have recently shown that an easterly shear can effectively destabilize equatorial Rossby waves and the convective heating can further amplify waves with the most unstable wavelength (about 4000 km) for reasonably realistic parameters. They also demonstrated that when the vertical easterly shear is confined to the NH, as in the case of the northern summer monsoon,
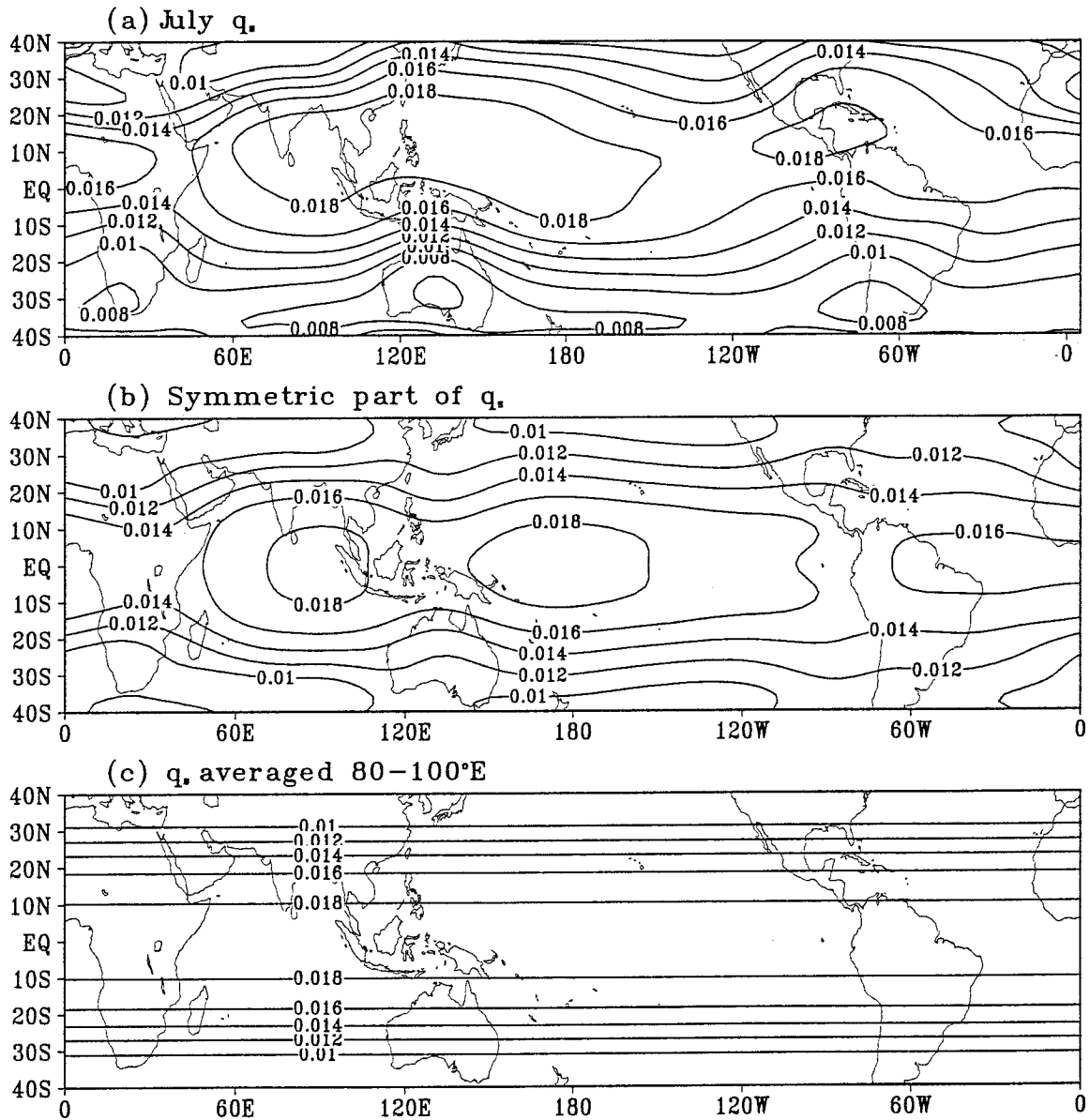
FIG. 3. (a) July mean specific humidity at 1000 hPa estimated using mean surface temperature and dewpoint temperature derived from ECMWF global analyses for the period 1979–92. (b) The symmetric (relative to the equator) part of the humidity field shown in (a). (c) The zonally uniform specific humidity derived by averaging the humidity field between 80° and 100°E shown in (b).

the structure of the gravest meridional mode can be remarkably modified. It is seen from Fig. 4 that the Southern Hemisphere cell of the equatorial Rossby wave is much weaker than its NH counterpart and is located much closer to the equator over the Indian Ocean sector. The Rossby waves emanating from the western Pacific around 150°E contain a much stronger northern cell (Figs. 4c,d). The corresponding southern cell occurs with a significant amplitude after its NH counterpart intensifies over southeast Asia at day 18 (Fig. 4e). Thereafter, both cells move westward, with strengthening of the southern cell (Fig. 4f). By day 26 the northern cell weakens rapidly, whereas the southern cell in-

itiates a new equatorial perturbation that then moves eastward along the equator (Fig. 4g). This starts another cycle that spans from day 28 to day 56 and displays an evolution similar to that of the previous cycle.

It is worthwhile to inspect time–latitude cross sections of the precipitation rate in order to detect the meridional propagation of the model low-frequency disturbances. Figure 5 shows six longitudinal profiles over the Indian and western Pacific Oceans. Over the Indian Ocean and South China Sea (Figs. 5a–c), there appears to be northward "propagation" of the precipitation area in the first two weeks. However, the phase speed is about 2° latitude per day, much faster than observed. The rapid northward
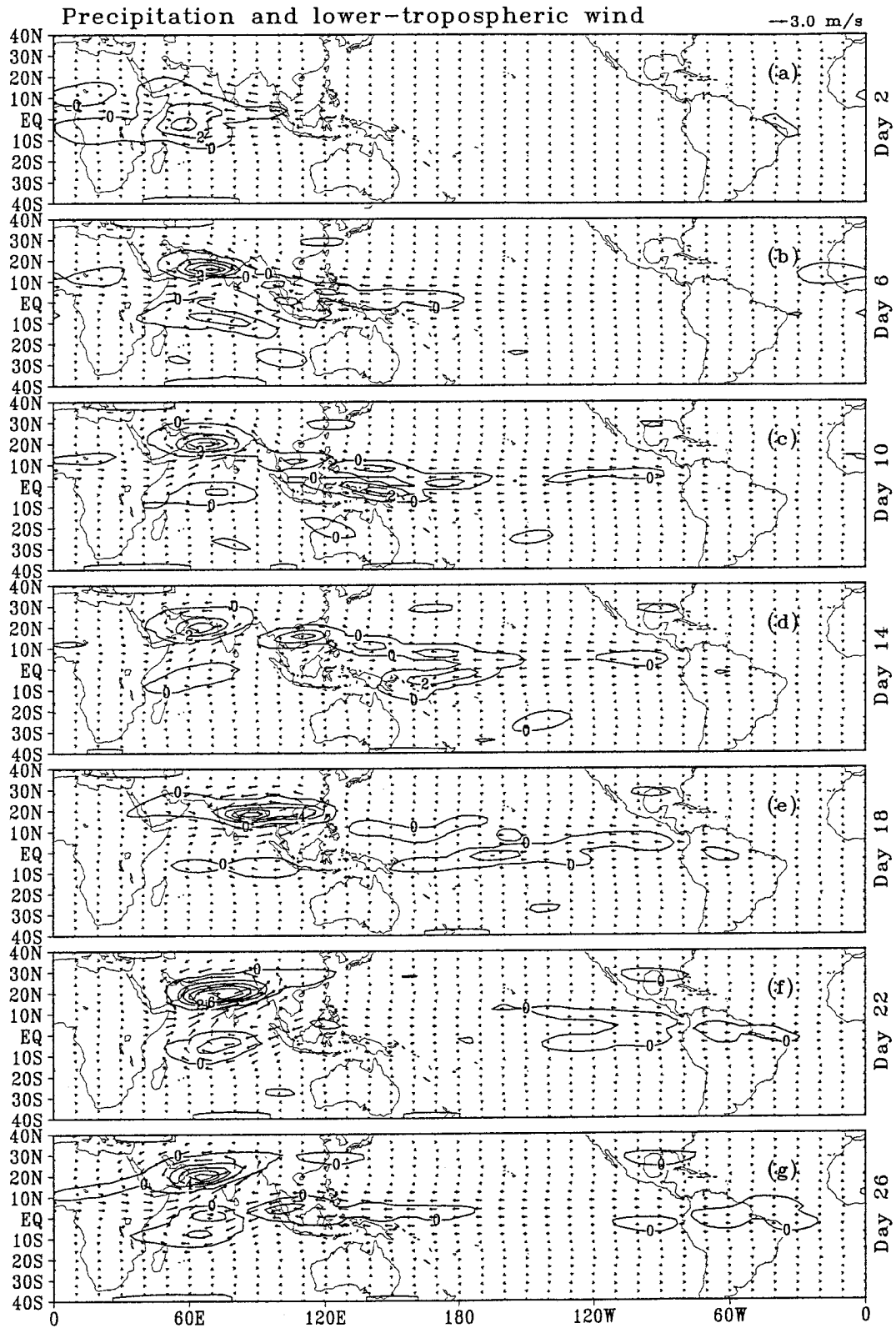
FIG. 4. Sequential maps of the lower-tropospheric winds and precipitation rate (contour interval is 2 mm day^{-1}) in the control experiment (expt 1).
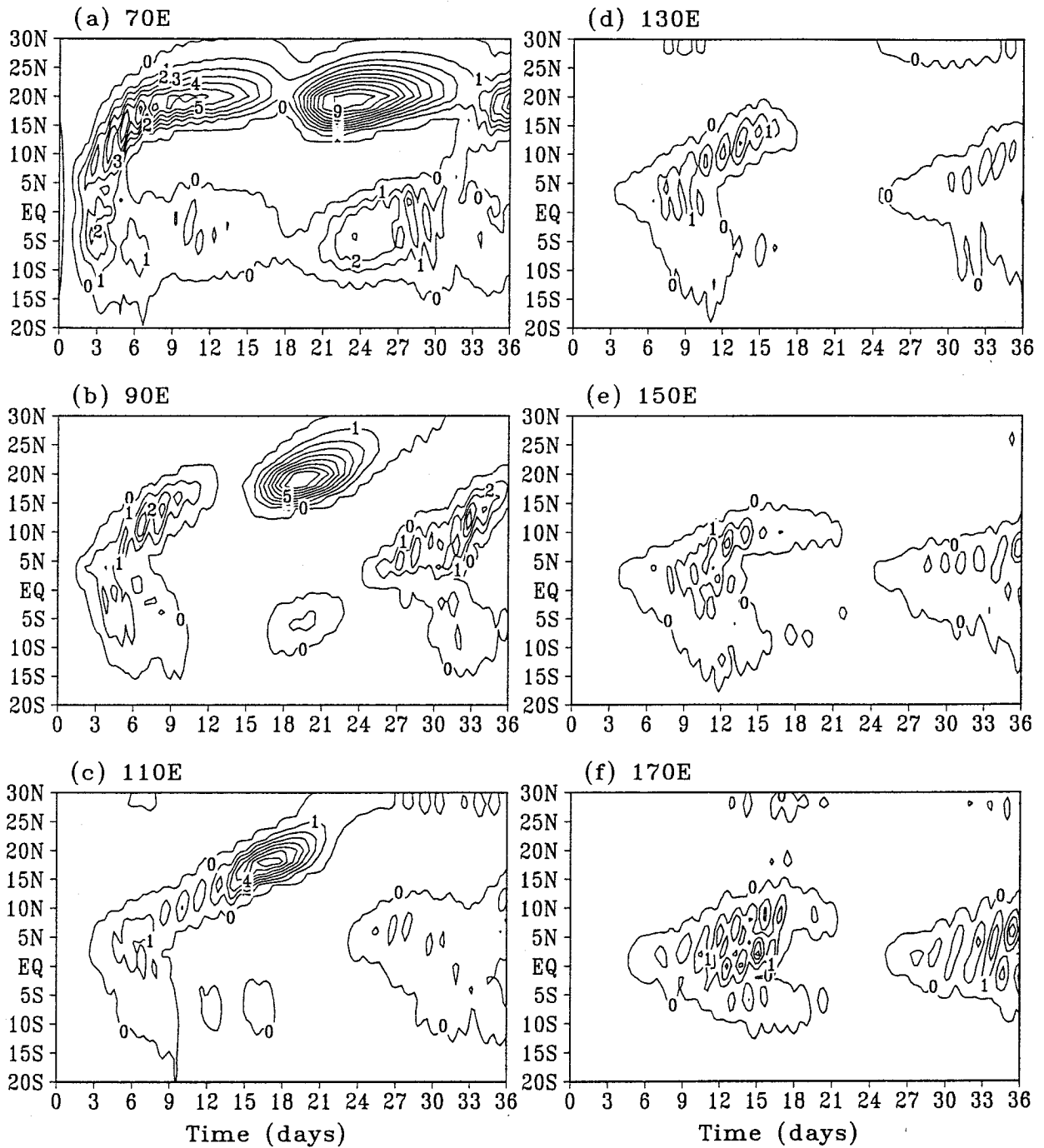
FIG. 5. Time–latitude diagrams of precipitation rate at (a) 70°E, (b) 90°E, (c) 110°E, (d) 130°E, (e) 150°E, and (f) 170°E for the control experiment. Contour interval is 1 mm day⁻¹.

shift of convection anomalies in the model simulation appears to be directly associated with the equatorial Kelvin–Rossby wave packet, which has a horseshoe shape convection "front" formed by the equatorial Rossby waves emanating from it. The convection front tilts northwestward from the equator to 20°N, resulting in a northward propagation component as the entire wave

packet migrates eastward. To the east of 150°E, the precipitation is confined to the equatorial region between 10°N and 10°S (Figs. 5e,f). It suggests that the excitation of Rossby waves originates from about 150°E.

To better display the equatorial eastward and off-equatorial westward propagating disturbances and their links, we present time–longitude diagrams along the
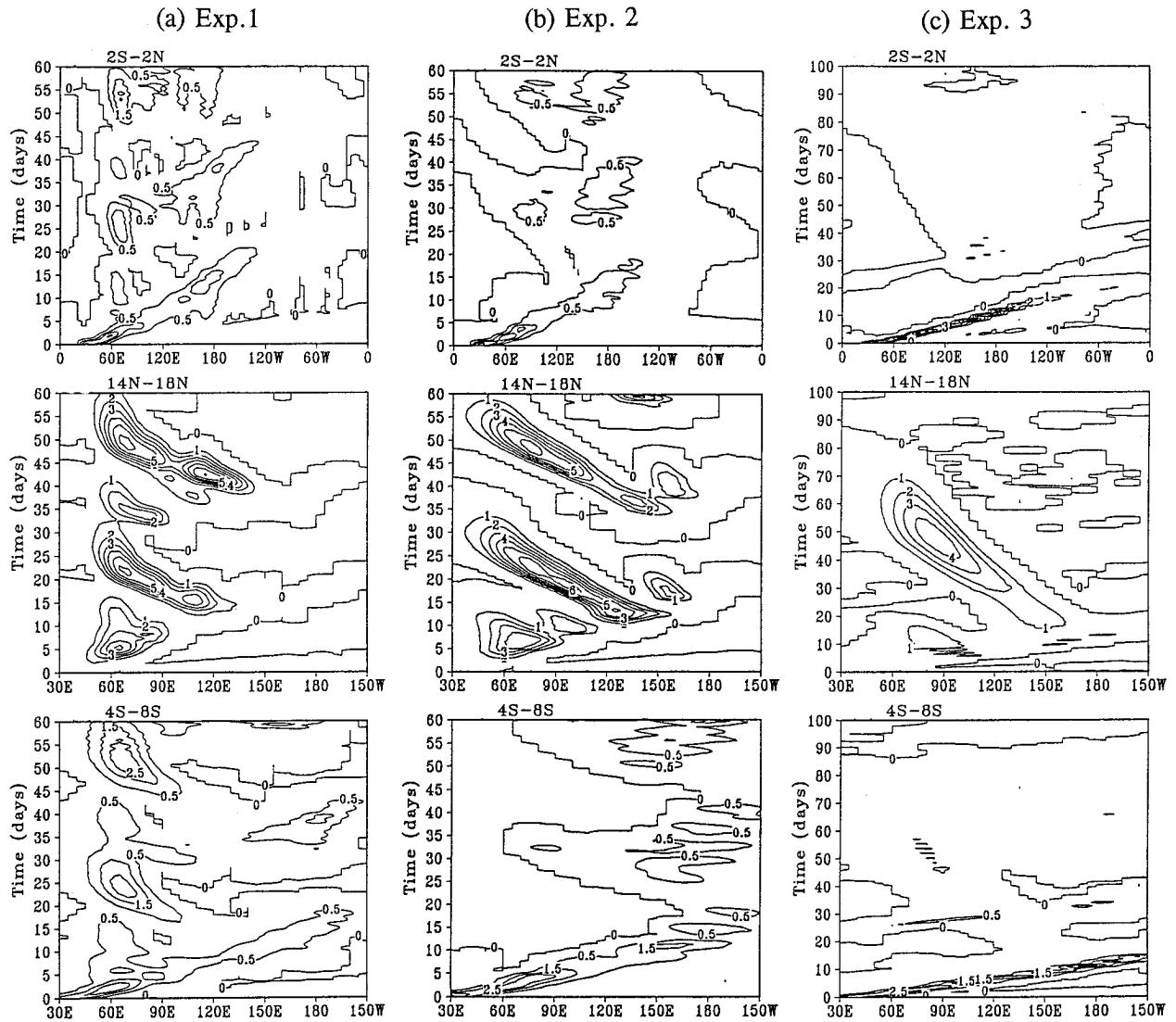
(a) Exp.1 (b) Exp. 2 (c) Exp. 3

FIG. 6. Time-longitude cross sections of precipitation rate along the latitude bands 2°S–2°N (upper panels), 14°–18°N (middle panels), and 4°–8°S (lower panels) simulated in (a) expt 1, (b) expt 2, and (c) expt 3, respectively.

equator at 2°S–2°N, 16°N, and 6°S, respectively (Fig. 6). The two off-equatorial latitude bands are located at the central latitudes where the northern and southern cells of Rossby waves respectively attain maximum strength. The zonal movement of the disturbances in the control experiment is shown in Fig. 6a. Along the equator, precipitation centers migrate eastward, with larger rainfall rates occurring over the equatorial Indian Ocean and western Pacific, where moisture content is high. The precipitation anomalies do not travel around the entire Tropics; rather, they decay rapidly after crossing the dateline. Whereas the eastward propagation dominates in the equatorial zone, the westward migration of the disturbances dominates between 14°N and 18°N. The westward propagation mainly occurs from about 140°E to 50°E with an averaged westward phase speed of about 7 m s^{-1}. Note that the active Rossby wave emanation

from the western Pacific and the subsequent intensification over the monsoon region occur when the equatorial disturbances arrive at the date line and are about to weaken. Along 4°–8°S, the eastward propagation associated with the equatorial convective complex remains clear. In addition, westward propagation is found from 110°E to 50°E from day 16 to day 25. Its generation follows the strengthening of the corresponding NH cell of the Rossby wave. Its subsequent movement and intensification concur with its NH counterpart as well. There is an obvious link between the off-equatorial westward and equatorial eastward propagations during the period from day 25 to day 30. It implies that as the westward moving disturbances stall and abate near 50°E, a new near-equatorial disturbance is reinitiated over the equatorial Indian Ocean. The scenario then repeats in a quasiperiodic manner.
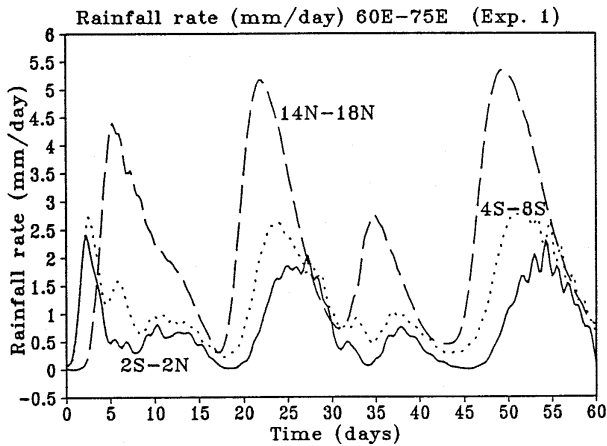
FIG. 7. The rainfall rate simulated in the control experiment over the Indian Ocean sector between 60°E and 75°E. The solid, dashed, and dotted lines represent the rainfall rate averaged over the latitude ranges 2°S–2°N, 14°–18°N, and 4°–8°S, respectively.

TABLE 2. Numerical experiment design.

Mean flow (July)	$\bar{q}_s$		
	Fig. 3a	Fig. 3b	Fig. 3c
No	Expt 3		Expt 4
$\bar{u}(y,z), \bar{T}(y)$	Expt 2		
$\bar{u}, \bar{v}, \bar{w}, \bar{T}$	Expt 1	Expt 5	Expt 6

Although the reinitiation of equatorial disturbances is a robust, easily reproducible feature appearing in our numerical simulations, we have not found its observational counterpart in the literature. To be cautious, let us further explore this process by focussing on the longitude sector between 60°E and 75°E, where the equatorial disturbances develop around day 26. Figure 7 shows that the northern cell of the Rossby wave at 14°–18°N reaches a maximum strength (as indicated by the precipitation rate) first around day 22, which is followed by the maximum strength of its southern cell on day 24 and, finally, that of the equatorial disturbance on day 27. Using the rainfall rate as an indicator of the wave available potential energy (APE) generation rate associated with the heating process, one finds that during the period of days 23–26, APE generation for the $n = 1$ (n is an index for the meridional modes) Rossby wave component decreases while that for the Kelvin wave component increases (figure not shown).

The model low-frequency disturbances display an evident tendency of being trapped in the Northern Hemisphere summer monsoon domain. The life cycle of the model disturbances is responsible for sustaining summer intraseasonal oscillation on a timescale of about 30 days. In the next two sections we will explore the dynamical factors that are responsible for the life cycle of the model disturbances.

4. Impacts of monsoon mean flows on ISO

In the control run (expt 1), the effects of monsoonal flows and inhomogeneous distribution of moisture sources are both included. To identify their respective contributions, we designed several controlled numerical experiments, as listed in Table 2. In all the experiments the model parameters and initial conditions are identical

to those used in expt 1 (see Table 1) except modifications in the mean flow or surface humidity field.

The impacts of mean monsoonal circulations can be assessed through comparison of the results obtained from expts 1–3, in which the surface humidity distribution is fixed (observed July mean), whereas the mean circulations are progressively simplified from a three-dimensional July mean (expt 1) to a modified July mean state containing only zonal flows with meridional and vertical shears (expt 2), and finally to a resting basic state (expt 3). The mean zonal flows in expt 2 are derived by averaging July mean zonal flows over the monsoon longitudes between 60°E and 150°E. The mean state in expt 2 has no mean meridional and vertical circulations; the zonal variation of mean zonal flow is also excluded for dynamical consistency. By comparing the results obtained from expts 1 and 2, one may identify the effects of the mean Hadley and Walker circulations, while by comparing the results of expts 2 and 3, one may identify the effects of vertical and meridional shears of mean zonal flows on the low-frequency waves and ISO.

Figures 6b and 6c show the time–longitude diagrams of precipitation rate simulated in expts 2 and 3, respectively. Comparing Figs. 6b (expt 2) and 6a (expt 1) reveals that without the mean Hadley and Walker circulations the equatorial Kelvin waves weaken over the western Pacific, the northern cell of the Rossby waves remains strong and more dominant over the equatorial mode while the southern cell of the Rossby waves is remarkably suppressed. As a result, the reinitiation of the equatorial disturbances over the Indian Ocean is much weaker and the equatorial MJO is evidently damped. On the other hand, the emanation of Rossby waves in the western North Pacific continues to be favored regardless of the weakening of the MJO along the equator. This is important for the maintenance of the ISO in the monsoon regions. It is concluded that the mean Hadley and Walker circulations play a vital role in the reinitiation of the disturbances over the equatorial Indian Ocean, but they are not critical to the Rossby waves' emanation in the western Pacific and development in the Asian monsoon regions.

Comparing Figs. 6c (expt 3) and 6b (expt 2) indicates that without the monsoonal zonal flows, the equatorial Kelvin waves exhibit an increased precipitation rate and a reduced zonal scale of the precipitation cell; the Rossby waves, however, weaken significantly with a much reduced speed (approximately 3 m s^{-1}) (note the dif-

ference in the time axis between Figs. 6b and 6c). Since the meridional shear of the zonal mean flow has a rather minor influence on the low-frequency waves (Wang and Xie 1996), the results here imply that the monsoon easterly vertical shear can remarkably enhance Rossby wave emanation in the western North Pacific and their development in the monsoon region, playing an essential role in sustaining ISO in the off-equatorial monsoon regions. It, however, tends to reduce the strength of the equatorial eastward propagating MJO.

It is interesting to notice that even without the mean monsoon flows, the moist Rossby waves continue to be excited in the western Pacific (Fig. 6c). What is responsible for the emanation of the Rossby waves in the western North Pacific? It turns out that the longitudinal variation of the surface humidity plays a key role, because when a zonally uniform humidity field is used (expt 4, see Table 2), the Rossby wave emanation completely disappears (figure not shown). This is because the zonal variation of the moist static energy source regulates the evolution of the equatorial MJO, which grows over the equatorial Indian and western Pacific Oceans but decays east of the dateline (Fig. 6c). When the equatorial convection decays, the Rossby waves decouple from the equatorial Kelvin wave and start to propagate westward. It follows that the moisture reduction in the central eastern Pacific favors Rossby wave emanation in the western North Pacific by suppressing equatorial convection that disintegrates the equatorial Kelvin–Rossby wave packet.

Note, however, that without the effects of the mean monsoonal flows the Rossby waves are weak and can no longer trigger the development of the equatorial disturbance over the Indian Ocean. Therefore, the model intraseasonal oscillation can not be sustained in both the equatorial and the summer monsoon regions.

5. The influences of the moisture distributions on ISO

The inhomogeneous surface humidity condition reflects, to a large degree, the variations in sea surface temperature and land surface moisture condition. The model moisture contents in the boundary layer and lower troposphere depend solely on the surface specific humidity. To identify its influence on summer ISO, one can compare expts 1, 5, and 6 (Table 2) in which the mean flows are fixed (observed July mean circulation), but the surface humidity conditions are progressively simplified from the July mean field in expt 1 (Fig. 3a) to the meridionally symmetric component of the July mean surface humidity field in expt 5 (Fig. 3b) and finally to the meridionally symmetric and zonally uniform humidity distribution in expt 6 (Fig. 3c). By comparing the results from expts 1 and 5, one may identify the effects of the asymmetric humidity distribution due to the warmest sea surface temperature occurring in the Northern Hemisphere, while by comparing the results

of expts 5 and 6, one may find out the effects of the longitudinal variation of the surface humidity on low-frequency waves and ISO.

For convenience of comparison we present, in Figs. 8a–c, the time–longitude diagrams of precipitation rates simulated in expts 1, 5, and 6, respectively. It is seen by comparing Figs. 8a and 8b that without the seasonally enhanced moisture content in the Northern Hemisphere the simulated precipitation rates along 14°–18°N are substantially reduced compared to those in the control run, indicating that the removal of the meridional asymmetry of the moisture distribution had considerably suppressed the Rossby wave development in the NH summer monsoon region. As a result, the southern cell of the Rossby waves along 4°–8°S is no longer discernible. Over the equatorial Indian Ocean no disturbance is reinitiated. This suggests that the moisture asymmetry due to northward shift of the thermal equator plays an important role in enhancing Rossby wave development in the Indian monsoon region and the reinitiation of equatorial disturbances over the Indian Ocean.

On the other hand, due to the slight increase of specific humidity over the equatorial eastern Pacific in expt 5 (Fig. 8b), the equatorial disturbances propagate farther east at a much faster speed about (25 m s^{-1}), traversing the entire equatorial band. A reinitiation of the equatorial disturbances in expt 5 appears over the western Pacific around day 30.

With a zonally uniform and meridionally symmetric mean specific humidity distribution (Fig. 8c), the model disturbances propagate eastward at a nearly constant speed (about 10 m s^{-1}). The eastward-moving equatorial disturbance is essentially a moist Kelvin–Rossby wave packet coupled by boundary layer moisture convergence-induced heating (Wang and Rui 1990b). The group speed of the wave packet (10 m s^{-1}) is slower than the individual moist Kelvin wave speed, which is about 15 m s^{-1} in the experiment. The slower energy propagation speed of the Kelvin–Rossby wave packet was first revealed in the study of Wang and Li (1994).

Even without the zonal variation of the moisture content, the strength of the equatorial wave packet is still longitude dependent: when passing through the Indian and western Pacific monsoon regions, the wave packet weakens. This is due to the mean flow effects. The result here agrees with that of Lau and Peng (1990). When the equatorial disturbances weaken over the Indian Ocean, there is a very weak indication of the generation of westward propagating Rossby waves over the Indian monsoon region. However, it is too weak to sustain the ISO. The 45-day oscillation in expt 6 is maintained by continuous eastward propagation of the equatorial Kelvin–Rossby wave packet (upper panel of Fig. 8c). This mechanism for the ISO is more relevant to the boreal winter ISO when the thermal equator nearly coincides with the geographic equator (so that the surface humidity is meridionally symmetric), favoring the maintenance of the MJO mode against dissipation.
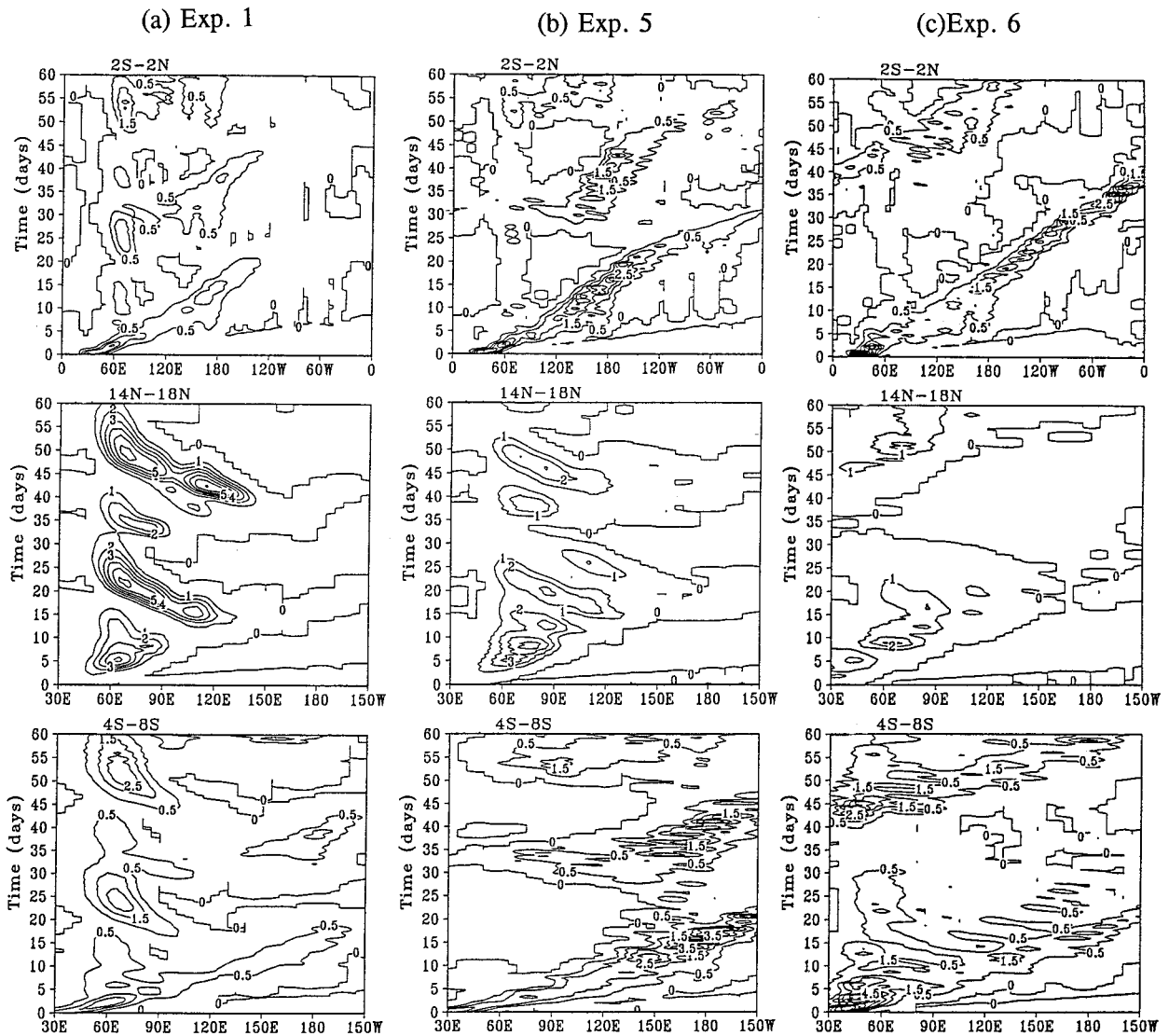
(a) Exp. 1　　　　　　　　　(b) Exp. 5　　　　　　　　(c)Exp. 6

FIG. 8. As in Fig. 6 except for (a) expt 1, (b) expt 5, and (c) expt 6, respectively.

Comparison of Figs. 8b and 8c indicates that the zonal variation of the surface humidity condition or moist static energy in the lower troposphere indeed plays a significant role in the emanation of Rossby waves in the western Pacific as inferred in the previous section.

6. Summary and discussion

This paper presents a simple model for the boreal summer intraseasonal oscillation (ISO). With realistic July mean basic flow and moist static energy distribution, the life cycle of low-frequency waves simulated in the model is highlighted by the schematic diagram in Fig. 9. The life cycle consists of four distinguished processes. 1) An initial semigeostrophic disturbance located at the east coast of Africa first moves eastward along the equator as a coupled Kelvin–Rossby wave

packet from the equatorial Indian Ocean to the Pacific. 2) As the equatorial disturbances rapidly decay in the eastern central Pacific, moist Rossby waves are excited in the western North Pacific and move northwestward toward the southeast Asian monsoon region. This bears close similarity to the movement of the low-frequency cloud and vorticity anomalies observed by Murakami et al. (1984), Nitta (1987), and Lau and Lau (1990). 3) The slowly westward propagating Rossby waves amplify while crossing southeast Asian monsoon region and exhibit strong asymmetry with respect to the equator due primarily to the effects of asymmetric distribution of monsoon easterly vertical shears. 4) As the strongly developed Rossby wave approaches the sinking dry air mass over the Middle East and North Africa, it starts to stall and decay, meanwhile reinitiating an equatorial convective disturbance that propagates eastward and
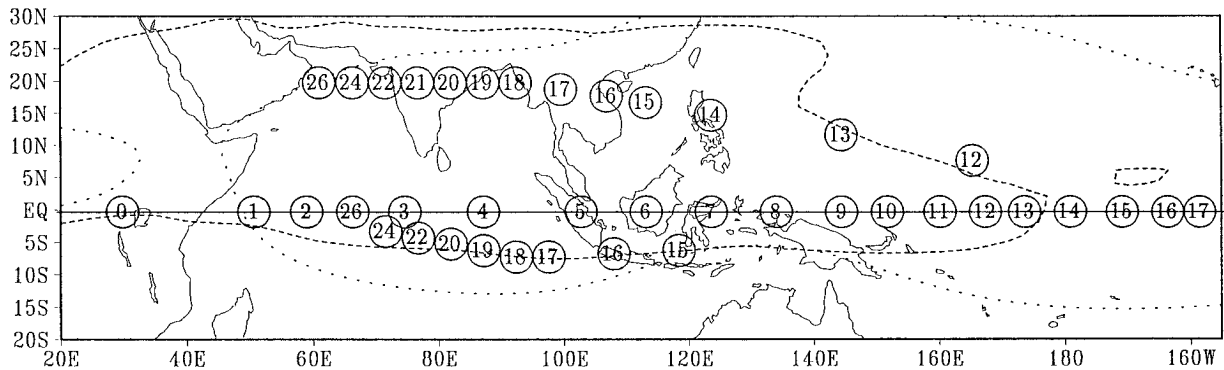
FIG. 9. The trajectory of the major precipitation centers in the control experiment with the encircled numers denoting the day of the model integration. Note that after day 15, there are two centers for each day located in both hemispheres that are associated with westward propagating equatorial Rossby waves. The dashed and dotted curves outline the contour lines of -4 m s^{-1} of July mean $U_{200} - U_{850}$ and 0.016 of July mean surface specific humidity, respectively.

starts the next cycle of the model low-frequency disturbances.

The life cycle of low-frequency disturbances provides a self-sustained oscillation mechanism for the boreal summer ISO. The life cycle is a result of the trapping of the low-frequency moist equatorial waves by NH summer monsoon mean flows and by the distribution of mean moist static energy. The oscillation period is determined by the sum of the time taken by the equatorial disturbance traveling from the Indian Ocean to the date line, the time taken by the westward propagating disturbances traveling from the western North Pacific to the Arabian Sea, and the time needed for emanation of Rossby waves in the western North Pacific and the reinitiation of equatorial disturbances over the Indian Ocean. With the Doppler shift effect of the mean flows, the time for low-frequency waves to complete the life cycle is on an order of one month. The actual intraseasonal oscillation has a broad band periodicity. The irregularity and regional difference may well be associated with episodic development, change of wave propagation speed due to local conditions, and modifications by other processes.

Three processes are critical for sustaining the model's northern summer ISO: the excitation of Rossby waves in the western North Pacific, the amplification of the Rossby waves over the Indian monsoon region, and the reinitiation of the equatorial disturbances over the Indian Ocean.

Why is the western North Pacific a favorable location for the emanation of Rossby waves? This is primarily due to the reduced moisture availability along with mean sinking motion (downdraft branch of Walker circulation) in the central eastern Pacific, which severely suppresses the convection, leading to disintegration of the equatorial Kelvin–Rossby wave packet. The high moist static energy supply and mean upward motion in the western North Pacific further favor the emanation of the Rossby waves from the decaying equatorial wave packet. The simultaneous weakening of the equatorial eastward-moving coupled Kelvin–Rossby wave packet and the generation of

off-equatorial Rossby waves imply an energy transfer from the Kelvin wave to the Rossby wave component.

What causes the development of the Rossby waves in the South Asian monsoon domain? The easterly vertical shear and seasonally enhanced moist static energy source play essential roles. Wang and Xie (1996) have shown that the meridional shear of zonal flow has rather moderate effects on large-scale equatorial waves, whereas the vertical shear of zonal flow has remarkable effects on westward propagating Rossby waves and Yanai waves because the vertical shear couples the barotropic and baroclinic modes and can resonantly excite the barotropic motion for Rossby waves. They also found that an easterly (westerly) shear confines the Rossby waves to the lower (upper) troposphere. This is because the excitation of barotropic mode depends on the sign of the vertical shear: the excited barotropic geopotential is precisely 180° out of phase with the geopotential thickness in an easterly shear, so that the superposition of the two vertical modes leads to a stronger (weaker) geopotential perturbation in the lower (upper) troposphere. Xie and Wang (1996) further demonstrated that in the presence of the boundary layer the easterly shear makes equatorial Rossby waves unstable because the enhanced lower-tropospheric perturbation motion induces stronger frictional moisture convergence and associated latent heating that favors instability. The localized easterly shear was shown to be capable of destabilizing and trapping the Rossby waves "in situ" and capable of changing the Rossby wave structure from symmetric to asymmetric with respect to the equator. The Rossby wave with a wavelength of 4000 km becomes the most unstable with its constant phase lines tilting horizontally (eastward with latitude) and vertically (against the shear). These features compare favorably with those of the boreal summer vorticity waves documented by Murakami et al. (1984) and Lau and Lau (1990). The theory can also well explain the behavior of the Rossby waves simulated in the present model.

How are the Indian Ocean near-equatorial distur-

bances reinitiated? We have demonstrated that the mean vertical circulation (the Hadley and Walker circulation) plays a critical role. In addition, whether the equatorial disturbances can be triggered depends also on the intensity of the off-equatorial Rossby waves and their asymmetry. In this sense, the monsoon easterly vertical shear and seasonally enhanced moist static energy source in the monsoon regions are also important. The mean flow asymmetry makes the Rossby waves of the lowest meridional mode extremely asymmetric: the northern cell is much more intense than the southern cell, while the southern cell is much closer to the equator. The intensification of the northern cell reinforces the southern cell. When the northern cell decays over the Arabian Sea, the southern cell appears to gain energy and generates a new equatorial disturbance. We speculate that this process implies an energy transfer from the moist Rossby wave to the equatorial Kelvin wave in the presence of the mean Hadley circulation and strong asymmetry in the Rossby wave structure.

Regardless of the notable success of the model in qualitatively reproducing observed features of the northern summer ISO, the model involves a number of crucial simplifications and approximations. Relatively heavy dissipation was used for achieving slowly growing low-frequency waves over the warm oceans, so that long-time integration is possible. The model dissipation can be reduced to normal by adjusting other parameters that control wave instability. The results here do not specifically rely on the heavy damping. The model serves merely as a mechanistic tool for illustrating an idealized intraseasonal oscillation scenario that could possibly occur during the northern summer. The hypothesis raised in this paper needs to be further investigated by analyzing observations and through numerical experiments with more sophisticated general circulation models. The precise mechanisms responsible for the energy transfer processes between equatorial Kelvin and Rossby waves require further theoretical studies. It also calls for further study to explore possible interactions between the tropical intraseasonal disturbances and various other processes such as cloud–radiation feedback and the ocean mixed layer thermodynamics in the future.

REFERENCES

Chen, T.-C., and M. Murakami, 1988: The 30–50 day variation of convective activity over the western Pacific Ocean with the emphasis on the northwestern region. *Mon. Wea. Rev.,* **116,** 892–906.

Emanuel, K. A., 1987: An air–sea interaction model of intraseasonal oscillation in the tropics. *J. Atmos. Sci.,* **44,** 2324–2340.

Goswami, B. N., and J. Shukla, 1984: Quasi-periodic oscillations in a symmetrical general circulation model. *J. Atmos. Sci.,* **41,** 20–37.

Hartmann, D. L., M. L. Michelson, and S. A. Klein, 1992: Seasonal variations of tropical intraseasonal oscillations: A 20–25-day oscillation in the western Pacific. *J. Atmos. Sci.,* **49,** 1277–1289.

Hendon, H. H., and M. L. Salby, 1994: The life cycle of the Madden–Julian oscillation. *J. Atmos. Sci.,* **51,** 2207–2219.

Krishnamurti, T. N., and D. Subrahmanyam, 1982: The 30–50 day mode at 850 mb during MONEX. *J. Atmos. Sci.,* **39,** 2088–2095.

Kuo, H.-L., 1974: Further studies of the parameterization of the influence of cumulus convection on large-scale flow. *J. Atmos. Sci.,* **31,** 1231–1240.

Lau, K.-H., and N.-C. Lau, 1990: Observed structure and propagation characteristics of tropical summertime synoptic scale disturbances. *Mon. Wea. Rev.,* **118,** 1888–1913.

Lau, K.-M., and L. Peng, 1990: Origin of low frequency (intraseasonal) oscillations in the tropical atmosphere. Part III: Monsoon dynamics. *J. Atmos. Sci.,* **47,** 1443–1462.

Lau, N.-C., I. M. Held, and J. D. Neelin, 1988: The Madden–Julian oscillation in an idealized GCM model. *J. Atmos. Sci.,* **45,** 3810–3832.

Madden, R. A., 1986: Seasonal variations of the 40–50 day oscillation. *J. Atmos. Sci.,* **43,** 3138–3158.

——, and P. R. Julian, 1971: Detection of a 40–50 day oscillation in the zonal wind in the tropical Pacific. *J. Atmos. Sci.,* **28,** 702–708.

——, and ——, 1972: Description of global-scale circulation cells in the tropics with a 40–50 day period. *J. Atmos. Sci.,* **29,** 1109–1123.

Murakami, T., 1980: Empirical orthogonal function analysis of satellite-observed outgoing longwave radiation during summer. *Mon. Wea. Rev.,* **108,** 205–222.

——, T. Nakazawa, and J. He, 1984: On the 45-day oscillations during the 1979 Northern Hemisphere summer. Part I: Phase propagation. *J. Meteor. Soc. Japan,* **62,** 440–468.

Nitta T., 1987: Convective activities in the tropical western Pacific and their impact on the Nothern Hemisphere summer monsoon. *J. Meteor. Soc. Japan,* **65,** 373–390.

Raymond, D. J., 1994: Convective processes and atmospheric circulations. *Quart. J. Roy. Meteor. Soc.,* **120,** 1431–1456.

Wang, B., 1988: Dynamics of tropical low-frequency waves: An analysis of the moist Kelvin wave. *J. Atmos. Sci.,* **45,** 2051–2065.

——, and H. Rui, 1990a: Synoptic climatology of transient tropical intraseasonal convection anomalies: 1975–1985. *Meteor. Atmos. Phys.,* **44,** 43–61.

——, and ——, 1990b: Dynamics of the coupled moist Kelvin–Rossby wave on an equatorial beta plane. *J. Atmos. Sci.,* **47,** 397–413.

——, and T. Li, 1993: A simple tropical atmospheric model of relevance to short-term climate variation. *J. Atmos. Sci.,* **50,** 260–284.

——, and ——, 1994: Convective interaction with boundary-layer dynamics in the development of a tropical intraseasonal system. *J. Atmos. Sci.,* **51,** 1386–1400.

——, and X. Xie, 1996: Low-frequency equatorial waves in vertically sheared zonal flow. Part I: Stable waves. *J. Atmos. Sci.,* **53,** 449–467.

Webster, P. J., 1983: Mechanisms of monsoon low-frequency variability: Surface hydrological effects. *J. Atmos. Sci.,* **40,** 2110–2124.

——, and S. Yang, 1992: Monsoon and ENSO: Selectively interactive systems. *Quart. J. Roy. Meteor. Soc.,* **118,** 877–926.

Xie, X., and B. Wang, 1996: Low-frequency equatorial waves in vertically sheared zonal flow. Part II: Unstable waves. *J. Atmos. Sci.,* **53,** 3589–3605.

Yasunari, T., 1979: Cloudiness fluctuations associated with the Northern Hemisphere summer monsoon. *J. Meteor. Soc. Japan,* **57,** 227–242.

——, 1981: Structure of an Indian summer monsoon system with around 40-day period. *J. Meteor. Soc. Japan,* **59,** 336–354.

Zhu, B. Z., and B. Wang, 1993: The 30–60 day convection seasaw between the tropical Indian and western Pacific Oceans. *J. Atmos. Sci.,* **50,** 184–199.